IEEE Access
Multidisciplinary | Rapid Review | Open Access Journal

Received July 15, 2021, accepted July 29, 2021, date of publication August 6, 2021, date of current version August 12, 2021.

Digital Object Identifier 10.1109/ACCESS.2021.3102991

An Efficient Approach of Improving Path Loss Models for Future Mobile Networks in Enclosed Indoor Environments

MOHAMED K. ELMEZUGHI, (Student Member, IEEE), AND THOMAS J. AFULLO, (Senior Member, IEEE)
Discipline of Electrical, Electronic and Computer Engineering, University of KwaZulu-Natal, Durban 4041, South Africa
Corresponding author: Mohamed K. Elmezughi (m.k.elmezughi@gmail.com)

ABSTRACT Path loss is the primary factor that determines the overall coverage of networks. Designing reliable wireless communication systems requires accurate path loss prediction models. Future wireless mobile systems will rely mainly on the super-high frequency (SHF) and the millimeter-wave (mmWave) frequency bands due to the massive available bandwidths that will meet projected users' demand, such as the needs of the fifth-generation (5*G*) wireless systems and other high-speed multimedia services. However, these bands are more sensitive and exhibit a different propagation behavior compared to the frequency bands below 6 *GHz*. Hence, improving the existing models and developing new models are vital for characterizing the wireless communication channel in both indoor and outdoor environments for future SHF and mmWave services. This paper proposes an efficient improvement of the well-known close-in (CI) free space reference distance model and the floating-intercept (FI) model. Real measured data was taken for both line-of-sight (LOS) and non-line-of-sight (NLOS) communication scenarios in a typical indoor corridor environment at three selected frequencies within the SHF band, namely 14 *GHz*, 18 *GHz*, and 22 *GHz*. The research finding of this work reveals that the proposed models have better performance in terms of their accuracy of fitting real measured data collected from measurement campaigns. In addition, this work studies the impact of the angle of arrival and the antenna heights on the current and improved CI and FI models. The results show that the improved models provide better stability and sensitivity to the change of these parameters. Furthermore, the mean square error between the models and their improved versions were presented. Finally, this paper shows that shadow fading's standard deviation can have a notable reduction in both the LOS and NLOS scenarios (especially in the NLOS), which means higher precision in predicting the path loss.

INDEX TERMS Path loss, 5*G*, 6*G*, channel modeling, millimeter-wave, propagation measurements, indoor environments, angle of arrival, antenna height, radio propagation.

I. INTRODUCTION

Era after era, the demand for higher mobile data traffic is exponentially increasing due to the tremendous revolution in technologies relying totally on mobile networks and their services. In 2019, Cisco reported that by 2022 the number of networked connections and devices would grow up to 28.5 *billion*, mobile-ready applications will reach up to 12.3 *billion* of them [1], [2]. Also, it was expected that by 2022 the overall mobile data traffic would be increased to approximately 77 exabytes per month, which is a seven-fold increase over the year of 2017 [2]. Another vital issue that will lead to more data needs is the current circumstances that the world faces nowadays, such as the Coronavirus pandemic that makes most of studying and work online, which leads to enormous use of the internet connection. Of course, this requires a massive amount of bandwidth [3]–[6].

Previously, the congestion of the spectrum below 6 *GHz* was enough to meet the existing systems' requirements. On the contrary, these bands will not meet the necessities of the fifth-generation (5*G*) cellular networks and many other applications due to their relative shortage in the bandwidth required [7]–[11]. Because of that, research has been done to adopt the frequency regime above 6 *GHz* as a promising solution to accomplish high peak data transmission rates up to multi gigabits per second with the contribution of complex

The associate editor coordinating the review of this manuscript and approving it for publication was Yi Ren.

modulation schemes and massive multiple-input multiple-output (Massive-MIMO) systems and other advanced techniques such as beamforming [12]–[18]. All these solutions together will satisfy the requirements of the 5*G* system. To the best of our knowledge, the research beyond 5*G* systems towards the sixth-generation (6*G*) cellular networks has already been started by escaping the current solutions of the 5G systems aiming for better performance [1], [19].

In June 2018, the first commercial 5*G* mobile communication standard (3GPP Release 15) was completed after many years of research and development. In the middle of 2019, some countries had already deployed 5*G* cellular networks. Meanwhile, the first 5*G*-enabled smart devices are now available on the market [1].

It is the norm to characterize and model the wireless communication channel in the frequency bands used (or expecting to be used) to better understand and accurately deploy the upcoming systems. Many researchers focused on this area by modeling the wireless channel's behavior using different ways: models based on theories, techniques such as ray-tracing, and measurement campaigns. The latter looks promising because of its accuracy and reliability since the measurements are in real environments and communication scenarios.

It is widely known that when a wireless communication system sends signals from the transmitting antenna(s), the wireless signals will have a reduction of their power as they travel through the wireless communication channel to the receiving antenna(s). This signal loss is well-known as path loss, which is the dominant component of the large-scale fading effects. The path loss is a vital component that must be modeled accurately to have reliable system design and link budget analysis. Moreover, the knowledge of the path loss provides statistically averaged (space and time) radio channel conditions. Consequently, researchers need to present more accurate path loss prediction models that can precisely describe the reduction of the wireless signal levels and accurately fit the real measured data collected in different indoor and outdoor environments over a wide range of frequency regimes. The reason behind the inability of the traditional models to be reliable models for the super-high frequency (SHF) and the millimeter-wave (mmWave) frequency bands and beyond is the significant sensitivity of the signals at these frequency bands to the propagation mechanisms in the communication channel. As an example, the mmWave signals provide substantial path loss values in the first meter away from the transmitting antenna and have a significant penetration loss through solid materials such as concrete walls [5], [20]–[23].

In general, the path loss can be modeled deterministically (theoretically), empirically (statistically), or stochastically [24]. The best understanding of the wireless channels' propagation characteristics can be done based on measurement campaigns in propagation's real environments [24]. In this study, we adopted measurement-based (semi-deterministic) models to predict the path loss taking into account the propagation mechanisms such as reflections and diffractions and the wave-guiding effect that occurs mainly in enclosed indoor environments such as corridors.

Recently, most research aimed to characterize and model the wireless channel has focused on specific path loss models because of their suitability, such as the close-in (CI) free space reference distance, floating-intercept (FI), and/or alpha-beta-gamma (ABG) model [25]–[45]. The improvement of these models in the literature was based on a consideration of some factors like cross-polarization discrimination (XPD), taking into account the mismatching of the antennas' polarization as in the models named CIX and ABGX models, which are an improvement of the CI and ABG models, respectively [23], [24]. Another improvement of the CI model is by presenting the path loss exponent (PLE) term as a frequency-dependent factor, as in the CIF model [23], [39], [46]–[48]. The last two factors (frequency-dependent PLE and XPD) were considered in one model called the CIFX model [23]. In [49] and [50], a dual-slope CI path loss model was presented. This model provides higher precision in predicting the path loss than the standard CI model. Note that all these improvements can be implemented easily on the FI and ABG models. Other improved models based on other different concepts can be found in [20], [27], [47], [51]–[53]. However, the question that has motivated this research is, *how can we improve the accuracy and reduce the standard deviation of the shadow fading of these standard path loss models without adding parameters that depend on something else like antennas' height or the XPD?*.

This question is answered through a fundamental principle: *any linear equation is a polynomial equation with zero coefficients in higher orders*. It is well-known that the standard path loss models (such as the CI and FI models) are a linear equation of the path loss as a function of the logarithmic scale of the separation distance between the transmitting and the receiving antennas. We incorporate an additional parameter to make these models a function of the transmitter-receiver (Tx-Rx) separation distance's squared logarithm. This adopted improvement is simple (in the improved models' equations, the proposed additional parameter that improves the standard models does not depend on anything like frequency and antenna height, etc.) and provides more precision in predicting the path loss, as will be proved in Section IV.

Many comparative studies between the existing path loss prediction models show the CI and FI models' preference over other models like the ABG model [23], [39], [54], [55]. The CI and FI models offer a precise estimation of the large-scale path loss as a function of the 3*D* Tx-Rx separation distance over the SHF and mmWave frequency regimes [24], [41], [55]. Hence, we hereby propose to further improve these two models while avoiding a significant increase in the models' complexity to be used by engineers in the wireless system design and calculations of the link-budget since the total number of the improved models' parameters is within a suitable range as other well-known models such as the ABG model have.

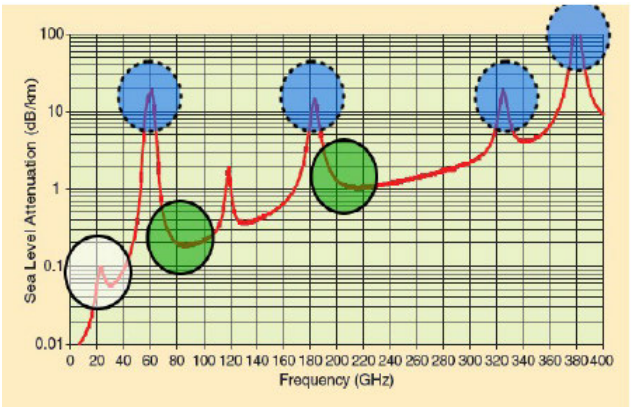

FIGURE 1. The air's attenuation at different frequency bands [35]. The white circle shows a minor attenuation of the low 5*G* frequency bands. Attenuation levels that are similar to the 4*G* cmWave bands are displayed in the green circles. The blue circles show high attenuation peaks; such bands are thus ideal for indoor communications with a minimal range.

The rest of this paper is organized as follows. In section II, a detailed derivation of the adopted path loss prediction models and their improvements are introduced and discussed. The measurement setup and environment are described in section III. The results and discussions of this research work are presented in section IV. Finally, section V draws the main conclusions and future aspects of this research.

II. LARGE-SCALE PATH LOSS PREDICTION MODELS

Generally, all path loss prediction models can be derived from Friis's equation [54], [55]:

$$FSPL(f, d) = (\frac{4\pi df}{c})^2, \quad (1)$$

where d is the Tx–Rx separation distance (in *meters*), f is the frequency of the propagated signal (in *Hz*), and c is the speed of light in the free space, which approximately equals to 3×10^8 m/s. This simple equation in the linear scale (absolute numbers) shows that the path loss between two isotropic antennas aligned on boresight toward each other is mainly a function of the operating frequency and the Tx-Rx separation distance. As presented in Eq. (1), the path loss is distance- and frequency-dependent; the increase in the frequency or the distance will produce higher path loss values. However, this is true when the wireless channel is in free space. In reality, the wireless channel's problems such as attenuation, interference, distortion, and noise in the communication schemes have random behavior. For example, Fig. 1 represents the attenuation in the air at different frequency bands in *GHz*. It is clear from the figure that the attenuation of the air does not follow a specific behavior. This means that some low frequencies have large path loss values in outdoor environments because of air attenuation and atmospheric absorption. This issue and many other problems have accelerated the research to cover all frequency bands by conducting measurement campaigns in typical indoor and outdoor environments to have reliable semi-deterministic channel models.

It is more convenient to present the path loss equations in the logarithmic scale. Hence, Eq. (1) can be written as follows:

$$FSPL(f, d)[dB] = 32.4 + 20\log_{10}(f) + 20\log_{10}(d). \quad (2)$$

The value 32.4 comes from $10\log_{10}(\frac{4\pi\times10^9}{c})^2$, and the value 10^9 is to have values of frequencies directly in *GHz* (i.e., f in Eq. (2) is the operating frequency in *GHz*). The variable d in the previous equation represents the Tx-Rx separation distance in *meters*.

The existing path loss models can be categorized as single-frequency (like the CI and FI models) or multi-frequency (like the ABG model). For single-frequency models, the term $20\log_{10}(f)$ is constant and can be added to the first term of Eq. (2). The result is a constant term that depends on the value of the frequency (single-frequency path loss models have a pure dependence on the frequency presented as a parameter). The representation of this parameter differs from one model to another. Let us name this parameter k_1. The term $20\log_{10}(d)$ is basically 2 times the distance in the logarithmic scale, where the value 2 is the free space path loss exponent (FSPLE), which indicates that the path loss changes with the square of the Tx-Rx distance in the free space. However, this value will change significantly, depending mainly on the medium's nature between the Tx and Rx. In general, it will be easier to denote it as k_2. Hence, Eq. (2) can be simplified as:

$$PL(d)[dB] = k_1 + k_2 \times 10\log_{10}(d), \quad (3)$$

where the coefficient k_1 is measured in *dB*, and k_2 is *unitless*. It is clear from the previous equation that the power of the propagated signal decreases by $\frac{1}{d^{k_2}}$. This means that higher values of k_2 will lead to stronger dependency of the path loss on the separation distance between the Tx and Rx. Depending on the techniques used to evaluate the values of these coefficients, different path loss models exist. This paper adopted from those several models in the literature two well-known path loss models, the CI and FI models, and our improvement on these models. The parameters of these semi-deterministic models are based on the real measured values of the received signal levels collected from measurement campaigns. The received signal power at the Rx side mainly depends on the strength of the transmitted signal (P_t), the path loss of the propagated signal (PL), and the gain of the transmitting and the receiving antennas (G_t and G_r), as presented in Eq. (4):

$$P_r(d)[dBm] = P_t - PL(d) + G_t + G_r. \quad (4)$$

In the previous equation, $P_r(d)$ and P_t are in *dBm*, G_t and G_r are in *dBi*, and $PL(d)$ is in *dB*.

A. THE CLOSE-IN (CI) FREE SPACE REFERENCE DISTANCE PATH LOSS PREDICTION MODEL

The CI model can be written from Eq. (3) by replacing k_1 by the value of the free space path loss at the operating frequency

(f) and the reference distance (d_0), and replacing k_2 by the *PLE* (n) as described in the following equation:

$$PL^{CI}(d)[dB] = FSPL(f, d_0) + 10n\log_{10}(d) + X_{\sigma}^{CI}, \quad (5)$$

where X_{σ}^{CI} is a Gaussian random variable with zero mean and a standard deviation σ in dB [6]. This term represents the shadow fading (SF), representing the large-scale fluctuations of the path loss values because of obstructions and other random propagation effects [56]. Having fewer values of the SF standard deviation means that the path loss models are more accurate. The SF's importance for researchers and engineers lies in the fact that it can establish standards that include large-scale fading statistical models without detailed knowledge of the characteristics of a site-specific environment [6].

In this work, we adopted the physically-based reference distance to be 1 m for the reason that the wireless signals at the frequency bands above 6 GHz exhibit significant path loss values in the first meter of the propagation away from the transmitting antenna [29]. Also, it will be easier to compare our work with other works as most of the researches in the open literature use 1 m reference distance. The free space path loss expressed in the dB scale at a reference distance $d_0 = 1$ m is given by:

$$FSPL(f, 1m) = 10\log_{10}(\frac{4\pi f}{c})^2. \quad (6)$$

Note that the CI model depends on one main parameter to be optimized, which is the *PLE* (n). The dependency of the path loss model on the 3D Tx-Rx separation distance is characterized by this unitless parameter (*PLE*). This model depends on a physical anchor that catches path loss near the transmitting antenna. It is clear that the CI model has an intrinsic dependency on the frequency of propagation that exists in the FSPL term. This term's values vary from 48 to 82 dB when the frequency range is between 6 and 300 GHz, respectively. The CI model is suitable for single- and multi-frequency situations and can estimate the path loss from both co- and cross-polarization cases [57].

The minimum mean square error (MMSE) technique is used to optimize the CI model's parameter (i.e., the PLE). Using this approach, we can achieve the least error of fitting the real measured data by minimizing the SF standard deviation.

B. IMPROVED CI PATH LOSS PREDICTION MODEL

To predict the path loss with more accuracy and sensitivity to the small changes of the propagation environments, we add an independent parameter to the CI model's equation. The improved model has two terms that depend on the 3D Tx-Rx separation distance. This means that the path loss exponent principle exists in two parameters (n_1 and n_2), as presented in the following equation:

$$PL^{Imp.\ CI}(d)[dB] = FSPL(f, d_0) + 10n_1\log_{10}(d) + 10n_2(\log_{10}(d))^2 + X_{\sigma}^{Imp.CI}, \quad d > 1m, \quad (7)$$

where n_1 and n_2 are the first order and second order of the *PLE*, respectively. This improvement of the CI will increase the opportunity to fit the real measured data collected from measurement campaigns and present more details in characterizing the wireless channel. Changing the environment where the signal can propagate, or the propagation's communication scenario (LOS or NLOS, etc.) will lead to a notable change in the values of n_1 and n_2. To have the closed-form of these parameters, let us assume that $A = FSPL(f, d_0)$, $B = PL^{Imp.\ CI}(d)$, $D = 10\log_{10}(d)$, and $E = 10(\log_{10}(d))^2$, then, the SF of Eq. (7) can be expressed as:

$$X_{\sigma}^{Imp.\ CI} = B - A - n_1 D - n_2 E. \quad (8)$$

The SF standard deviation ($\sigma_{Imp.\ CI}$) can be determined from the experimental data using:

$$\sigma_{Imp.\ CI} = \sqrt{\frac{\sum (X_{\sigma}^{Imp.\ CI})^2}{N}}, \quad (9)$$

where N is the number of the Tx-Rx separation distances (i.e., the total number of the average path loss samples recorded). Now, we have to differentiate the numerator of Eq. (9) with respect to both n_1 and n_2 and equate the result to zero to have the optimum value of these parameters that will lead to the minimum value of the standard deviation as follows:

$$\frac{\partial}{\partial n_1}(\sum (B - A - n_1 D - n_2 E)^2) = 0, \quad (10)$$

$$\frac{\partial}{\partial n_2}(\sum (B - A - n_1 D - n_2 E)^2) = 0. \quad (11)$$

After the differentiation and simplification of the previous two equations, we have two linear equations which can be expressed as:

$$\sum D^2 n_1 + \sum (DE) n_2 = \sum (BD) - A \sum D, \quad (12)$$

$$\sum (DE) n_1 + \sum E^2 n_2 + = \sum (BE) - A \sum E. \quad (13)$$

The matrix form of the equations (12) and (13) can be written easily as:

$$\begin{bmatrix} \sum D^2 & \sum (DE) \\ \sum (DE) & \sum E^2 \end{bmatrix} \begin{bmatrix} n_1 \\ n_2 \end{bmatrix} = \begin{bmatrix} \sum (BD) - A \sum D \\ \sum (BE) - A \sum E \end{bmatrix}. \quad (14)$$

Finally, the closed-form of n_1 and n_2 can be found from the previous matrix.

C. THE FLOATING-INTERCEPT (FI) PATH LOSS PREDICTION MODEL

The FI model has been widely used in 3GPP and WINNER II standards [5], [23], [24], [48], [56]. It does not depend on the physical anchor point constraint that catches the path loss near the transmitting antenna. However, it depends on the mathematical curve that fits the measured path loss values. As a linear equation, the FI model has two parameters, which are the intercept (denoted by α) and slope (indicated by β) of the path loss line as presented in the following equation:

$$PL^{FI}(d)[dB] = \alpha + 10\beta\log_{10}(d) + X_{\sigma}^{FI}, \quad d > 1m, \quad (15)$$

where $PL_{FI}(d)$ is the path loss in dB, and X_{σ}^{FI} is a Gaussian random variable with zero mean and a standard deviation σ_{FI}. In the previous expression, both X_{σ}^{FI} and σ_{FI} are in dB. It is worth noting that the FI model's parameters are unlike the CI model (α is unlike FSPL, and β is unlike the PLE). However, the models have comparable overall performance in predicting the path loss with a preference of one over the other depending on the operating frequency as well as the environment and communication scenario of the wireless communication system [10], [57], [58].

D. IMPROVED FI PATH LOSS PREDICTION MODEL

In this model, we follow the same principle as we used for the improved CI model, which is adding an independent parameter that will be the coefficient of the square of the logarithm of the $3D$ Tx-Rx separation distance as presented in the following equation:

$$PL^{Imp.\,FI}(d)[dB] = \alpha + 10\beta_1 \log_{10}(d) + 10\beta_2(\log_{10}(d))^2 + X_{\sigma}^{Imp.FI}, \quad d > 1m, \tag{16}$$

As seen from Eq. (16), this model has three parameters to be known (α, β_1, and β_2). Using the MMSE approach and following the same derivation we used for the improved CI model, the solution matrix of these parameters can be expressed as:

$$\begin{bmatrix} N & \sum D & \sum E \\ \sum D & \sum D^2 & \sum (DE) \\ \sum E & \sum (DE) & \sum E^2 \end{bmatrix} \begin{bmatrix} \alpha \\ \beta_1 \\ \beta_2 \end{bmatrix} = \begin{bmatrix} \sum B \\ \sum (BD) \\ \sum (BE) \end{bmatrix}, \tag{17}$$

where $B = PL^{Imp.\,FI}(d)$, $D = 10\log_{10}(d)$, and $E = 10(\log_{10}(d))^2$. The closed-forms of the parameters are found from the previous matrix. To validate the proposed models given in equations (7) and (16), we used real measured data of the path loss in a typical indoor corridor environment, as explained in the next section.

III. MEASUREMENT SETUP AND DATA COLLECTION METHOD

A detailed description of radio frequency (RF) propagation measurement campaigns conducted in a typical enclosed corridor environment is provided in this section. The corridor exists on the 5th floor of the Discipline of Electrical, Electronic, and Computer Engineering, University of KwaZulu-Natal, Howard College Campus, Durban 4001, South Africa.

Before beginning the measurement campaigns, we ensured that no other transmissions on the same experimental radio frequency bands existed. Also, the measurement system was carefully calibrated, and the measurements were repeated and averaged to ensure high-quality data collection.

The wireless propagation channel is a corridor environment with dimensions of 30, 1.4, 2.63 *meters* as a length, width, and height. Both sides of the corridor are made of bricks and dry concrete with wooden doors to offices on one side and an elevator and a staircase on the other side. It is worth noting that these indoor corridors can be approximated as a rectangular air-filled waveguide with dimensions immense compared to signals' wavelength. This environment is crucial and commonly used for many indoor applications.

The antennas used in this experiment are vertically-polarized with directional radiation patterns. The Tx antenna's height was 160 and 230 *centimeters* above the floor level, while the Rx height was 160 *centimeters*; which are the average antenna heights for these indoor environments that are adopted by many researchers [29], [59]–[61]. When the Tx antenna height was 230 *centimeters* above the floor level, we down tilted the Tx antenna to ensure that both antennas are aligned on boresight for all the Tx-Rx measurement places in the LOS communication scenario. Three frequencies in the SHF band were considered in this work: 14, 18, and 22 *GHz*. Both antennas were pyramidal horn antennas with half-power beamwidth values between 13 and 19.2 *degrees* and a directional gain ranging between 19.5 and 22.1 *dBi* at the operating frequencies. Throughout the campaigns, the intent was to place the Tx at one end of the corridor and moving the Rx away from the Tx, having a Tx-Rx separation distance of $2-24$ *meters* with an incremental step of 2 *meters* a time. The reference Tx-Rx distance was 1 *meter*, as is recommended by most research experts in this field [62]–[66]. Note that to satisfy the far-field requirements, the distance from the Tx should be much greater than the wavelength of the lowest operational frequency, which already exists since the wavelength of the SHF signals is in the range of *millimeters*.

The measurements were performed under the conditions of LOS and NLOS communication scenarios. In the LOS scenario, both antennas were aligned on boresight, and there were no obstacles in the direct propagation path between them. In contrast, the Rx in the NLOS depends mainly on diffractions, reflections, and waveguiding mechanisms in the corridor environment since both antennas had no alignment on boresight. Throughout the measurements, the transmit power was fixed at 10 *dBm*. However, the received power level range was between -41.33 and -19.05 *dBm*. The angle of departure (AoD) was set at 0 *degree*, while the angle of arrival (AoA) was in the range of $0 - 360$ *degrees* with an incremental step of 10 *degrees* a time.

A Rohde and Schwarz SMF 100A signal generator working in continuous-wave (CW) mode was applied to feed the transmitting antenna. The measured results are collected by means of a Rohde and Schwarz FSIQ 40 Signal Analyzer. This receiving equipment records 500 data sets of received signal strength (RSS) per each AoA and Tx-Rx separation distance. The RSS data were averaged to ensure accurate detection of the CW signals. Both signal generator and signal analyzer were directly connected to the antennas through coaxial cables. Since the path loss is the difference value between the Tx and Rx power, taking into account the antennas' gain and the coaxial cables' loss, the measured path loss PL_m is calculated by:

$$PL_m[dB] = P_t - P_r + G_t + G_r - L_{cable}, \tag{18}$$

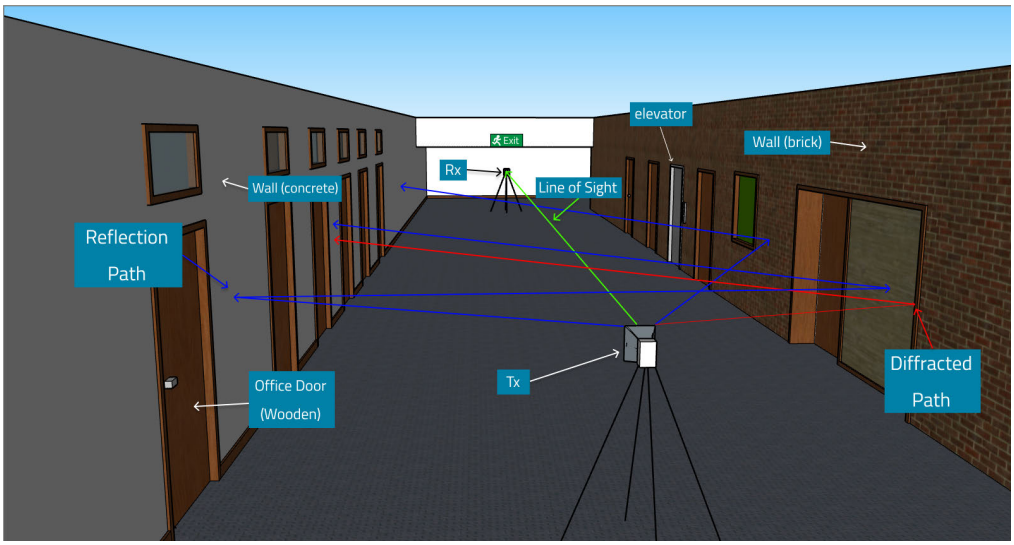

FIGURE 2. 3D floor plan of the indoor corridor environment.

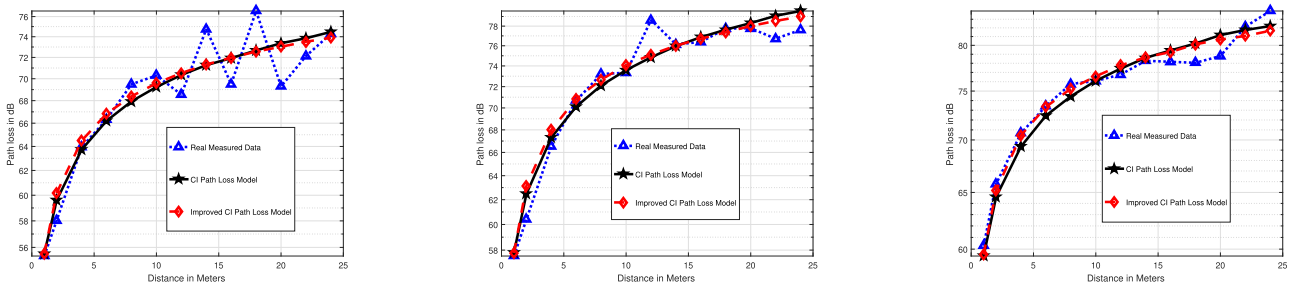

(a) $f = 14\,GHz$. (b) $f = 18\,GHz$. (c) $f = 22\,GHz$.

FIGURE 3. Comparison of measured path loss, the fitted CI model, and the improved CI model for the LOS results at 14, 18, and 22 *GHz*.

where L_{cable} is the total coaxial cable loss of the measurement system in *dB*. Fig. 2 represents the 3*D* floor plan of the indoor corridor environment. The parameters of the measurement setup used in this work are summarized in Table 1.

IV. RESULTS AND DISCUSSIONS

This section presents and discusses the main results obtained from this research work. It is presented in two subsections, each one compares a model with its improved version at the three frequencies (14, 18, and 22 *GHz*) for both the LOS and NLOS scenarios. Also, each subsection investigates the behavior of the models' parameters with the AoA and the antenna's height.

A. RESULTS AND DISCUSSIONS OF COMPARING THE CI WITH IMPROVED-CI MODELS

Fig. 3 depicts the real measured path loss, the CI model, and the Improved-CI model together for the LOS communication scenario at the three frequencies. It is clear from the figure that both models fit the measured path loss adequately and both have a comparable performance with a slight preference of the improved model. This also can be noted from Table 2 that presents the values of the models' parameters.

TABLE 1. Channel sounder specifications and parameters configuration.

Parameter	Configuration	Units
Center Frequencies	14, 18, and 22	GHz
Bandwidth	100	MHz
Transmission Signal	Continuous Wave	-
Tx and Rx Antennas	Direc. Horn Ant.	-
Tx Antenna Power	10	dBm
Tx Antenna Height	1.6 and 2.3	m
Rx Antenna Height	1.6	m
Tx and Rx Ant. Gain at 14 GHz	19.5	dBi
Tx and Rx Ant. Gain at 18 GHz	20.95	dBi
Tx and Rx Ant. Gain at 22 GHz	22.1	dBi
Tx and Rx Elev. HPBW at 14 GHz	19.2	Degrees
Tx and Rx Azim. HPBW at 14 GHz	18.4	Degrees
Tx and Rx Elev. HPBW at 18 GHz	15.6	Degrees
Tx and Rx Azim. HPBW at 18 GHz	15.4	Degrees
Tx and Rx Elev. HPBW at 22 GHz	13	Degrees
Tx and Rx Azim. HPBW at 22 GHz	15	Degrees
Tx and Rx Ant. Polarization	Vertical	-

Our proposed model minimizes the shadow fading's standard deviation at the three frequencies by 2.3%, 5.2%, and 10.7% at 14, 18, and 22 *GHz*, respectively. We note that the reduction of the standard deviation becomes higher as we go for high frequency bands. This is because the higher frequency bands suffer from many propagation effects and have higher path loss values than lower bands. From Table 2, for the CI model,

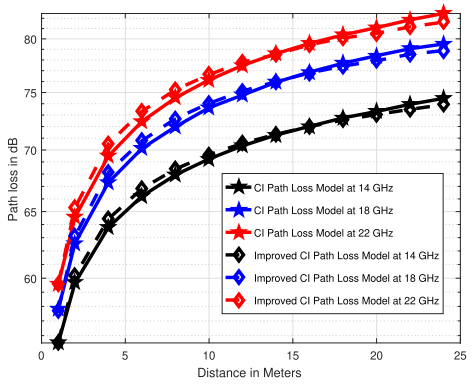

FIGURE 4. Directional large-scale path loss prediction models for the LOS communication scenario.

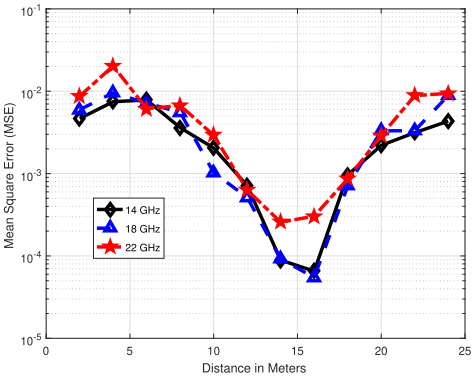

FIGURE 5. MSE between the CI and improved CI models in the LOS communication scenario.

the path loss exponent is directly proportional to the operating frequency. This leads to the general fact that higher frequency bands have higher path loss values. All the PLE's values are under the value of the FSPLE. The reason behind that is the constructive interference between the multipath signals which makes the PLE lower than 2. For the improved-CI model, as discussed previously, the concept of the PLE has split into two parameters (i.e., n_1 and n_2) as shown in Table 2. This technique gives the model more relaxation to accurately fit the measured data. It is clear that the values of n_1 are higher than the values of the CI model's PLE. However, all the values of n_2 are negative, which will compensate the increase of n_1 values and make the model following the measured path loss and counts all the possible signal effect. Fig. 4 offers a graphical view of both models (CI and improved-CI) together at 14, 18, and 22 *GHz* for the LOS communication scenario. We plotted the MSE curves between the CI and improved CI models with respect to the separation distance between the Tx and Rx for the LOS scenario as depicted in Fig. 5. It is worth noting that all the MSE values are in the range of 10^{-4} to 10^{-2} with lower values around 14 to 16 *meters* (near the breakpoint of the corridor) of the Tx-Rx separation distance.

In the NLOS communication scenario, as it is known, the receiving antenna relies mainly on reflection, diffraction and the effect of waveguiding in this enclosed environment for capturing the signals from the Tx. The CI model's PLE

TABLE 2. A comparison between the CI and Improved-CI models' parameters in the LOS scenario.

	$14\,GHz$	$18\,GHz$	$22\,GHz$
$PLE\ (n)$	1.37	1.58	1.66
$\sigma^{CI}_{min}[dB]$	2.19	1.53	1.31
n_1	1.61	1.87	1.99
n_2	−0.20	−0.24	−0.28
$\sigma^{Imp.CI}_{min}[dB]$	2.14	1.45	1.17

TABLE 3. A comparison between the CI and Improved-CI models' parameters in the NLOS scenario.

	$14\,GHz$	$18\,GHz$	$22\,GHz$
$PLE\ (n)$	2.07	2.38	2.26
$\sigma^{CI}_{min}[dB]$	5.98	6.87	6.86
n_1	5.09	5.86	5.69
n_2	−2.57	−2.97	−2.92
$\sigma^{Imp.CI}_{min}[dB]$	2.74	3.08	3.23

values here are 2.07, 2.38, and 2.26 at 14, 18, and 22 *GHz*, respectively. Note that because there is no direct dominant path from the transmitting to the receiving antennas, the values became notably high compared to the LOS results. However, they are still low compared to the communications in outdoor environments where the fluctuations of the propagated signals is much stronger. We find that in enclosed indoor environments such as corridors, the PLE values will not go much higher than the values of the FSPLE since the maximum percentage jump is in 18 *GHz* band by 16%. This frequency band (i.e., 18 *GHz*) has a higher sensitivity to the wireless channel effects than the others for the frequencies studied. The SF standard deviation of the CI model is seen to rise to more than the double in the NLOS scenario as shown in Table 3. This means that there is less precision in predicting the path loss in NLOS scenarios than the LOS ones. Nevertheless, the proposed model provides an attractive reduction of the standard deviation since it produces a minimum reduction of 3.24 *dB* (54.2% less) as can be seen in Table 3. This improvement is simple and highly efficient since almost all the communication methods for indoor environments are NLOS. The reason behind this improvement is the fact that the current statistical NLOS models cannot properly model the propagation mechanisms such as reflections and diffractions effects, which are captured better by the new parameter in our improved model. Again, all the values of the parameter n_2 are negative and n_1 values are larger than the PLE value for the NLOS scenario as the LOS one. Fig. 6 displays both models at the three selected frequency bands. From this figure, it is clear that the path loss curves of the improved CI model are away from the CI model's curves. The MSE between the CI and improved CI models are outlined in Fig. 7 for the NLOS scenario. The figure shows the increase in the MSE values compared to the LOS scenario since for the NLOS, the MSE values are in the range of 10^{-2} to 10^{0}.

The behavior of the CI and Improved-CI models' parameters with the AoA at 14, 18, and 22 *GHz* is presented in detail in Table 4, Table 5, and Table 6, respectively. From the Tables, it is clear that the PLE's minimum values occur when

TABLE 4. The behavior of the CI and Improved-CI models' parameters with the AoA at 14 *GHz* frequency band.

	30°	60°	90°	120°	150°	180°	210°	240°	270°	300°	330°
$PLE\ (n)$	2.0026	2.0950	2.0965	2.0954	2.1006	2.0604	2.1049	2.0968	2.0952	2.0832	1.9707
$\sigma^{CI}_{min}[dB]$	4.73	6.18	6.25	6.20	6.40	6.37	6.63	6.37	6.30	5.80	4.59
n_1	4.4763	5.1908	5.2955	5.2026	5.3150	5.1780	5.3981	5.3147	5.2882	5.0508	4.3108
n_2	−2.105	−2.635	−2.722	−2.644	−2.736	−2.653	−2.803	−2.738	−2.717	−2.525	−1.991
$\sigma^{Imp.CI}_{min}[dB]$	1.86	2.93	2.72	2.92	2.99	3.23	3.21	2.92	2.86	2.53	2.02

TABLE 5. The behavior of the CI and Improved-CI models' parameters with the AoA at 18 *GHz* frequency band.

	30°	60°	90°	120°	150°	180°	210°	240°	270°	300°	330°
$PLE\ (n)$	2.1836	2.3478	2.4074	2.4114	2.4166	2.3503	2.4205	2.4110	2.4048	2.4198	2.3712
$\sigma^{CI}_{min}[dB]$	4.42	6.20	7.10	7.31	7.36	7.24	7.52	7.18	6.99	7.65	6.56
n_1	4.5208	5.5663	6.0441	6.1024	6.1328	5.9643	6.1947	6.0495	5.9568	6.2216	5.7193
n_2	−1.989	−2.739	−3.095	−3.141	−3.163	−3.076	−3.212	−3.096	−3.023	−3.235	−2.849
$\sigma^{Imp.CI}_{min}[dB]$	1.61	2.52	3.08	3.35	3.38	3.47	3.53	3.25	3.13	3.72	2.89

TABLE 6. The behavior of the CI and Improved-CI models' parameters with the AoA at 22 *GHz* frequency band.

	30°	60°	90°	120°	150°	180°	210°	240°	270°	300°	330°
$PLE\ (n)$	2.2099	2.2585	2.2752	2.2747	2.2751	2.2523	2.2738	2.2775	2.2754	2.2542	2.2192
$\sigma^{CI}_{min}[dB]$	5.93	6.58	7.03	7.13	7.22	7.23	7.18	7.21	7.20	6.70	6.03
n_1	5.2224	5.5827	5.7903	5.8321	5.8638	5.8427	5.8460	5.8715	5.8624	5.6136	5.3165
n_2	−2.564	−2.829	−2.991	−3.027	−3.054	−3.056	−3.040	−3.059	−3.053	−2.859	−2.636
$\sigma^{Imp.CI}_{min}[dB]$	2.66	3.01	3.35	3.42	3.50	3.52	3.47	3.46	3.47	3.15	2.58

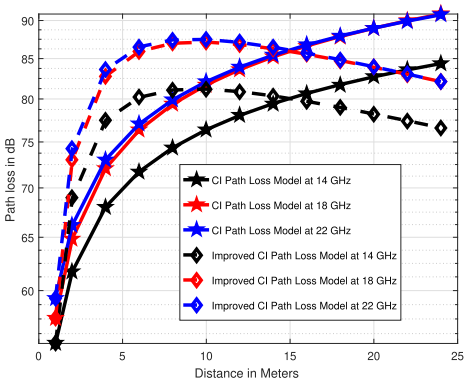

FIGURE 6. Directional large-scale path loss prediction models for the NLOS communication scenario.

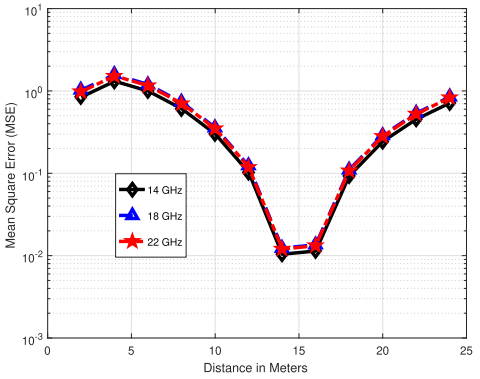

FIGURE 7. MSE between the CI and improved CI models in the NLOS communication scenario.

the AoA equals 30 and 330 *degrees*. The reason behind that is that at these AoA values, the Rx antenna is still aligned near the LOS path, and with the help of the propagation mechanisms discussed above, the PLE's value is minimized. The maximum PLE values occur at 150 and 210 *degrees* of the AoA. This shows that around these angles when the Rx is in the opposite direction of the Tx, the propagated signal will suffer from maximum path loss values before reaching the Rx antenna. Note that when the AoA is exactly 180 *degrees*, the PLE values are within a good range compared to other AoA because of the back loops of the Rx antenna's radiation pattern as can be seen from Fig. 8. These findings give an insight into what will happen in reality when the Tx or Rx orientations might not be known and how the wireless signals will be affected according to this issue in such enclosed indoor corridor environments. When we compare the three frequencies together, we observe that the fluctuations of the PLE values are 6.8%, 10.4%, and 3.1% at 14, 18, and 22 *GHz*, respectively. This means that the 22 *GHz* frequency band has an attractive behavior in terms of its stability to the AoA, which leads to accurate modeling of the wireless propagation channel in the NLOS communication scenario. For the SF's standard deviation values, the difference between the maximum and minimum values are 2.04, 3.1, and 1.3 *dB*. It is clear that the worst performance between the three frequencies is at 18 *GHz*. For our proposed model, since the concept of the PLE is divided into two parameters, it is clear from the Tables that it outperforms the CI regarding the sensitivity and stability of the model's parameters with the AoA.

Fig. 9 depicts the CI and improved-CI models' parameters at two different practical antenna heights (i.e., 1.6 and 2.3 *m*) for both the LOS and NLOS communication scenarios. Generally, the figure shows the increase of the parameters' values when the Tx antenna height is 2.3 *m* compared to 1.6 Tx antenna height because of the mismatching of the antennas' heights. Moreover, it can be seen from the figure that our proposed model provides more sensitivity to the antenna height and capture more accurately the wireless

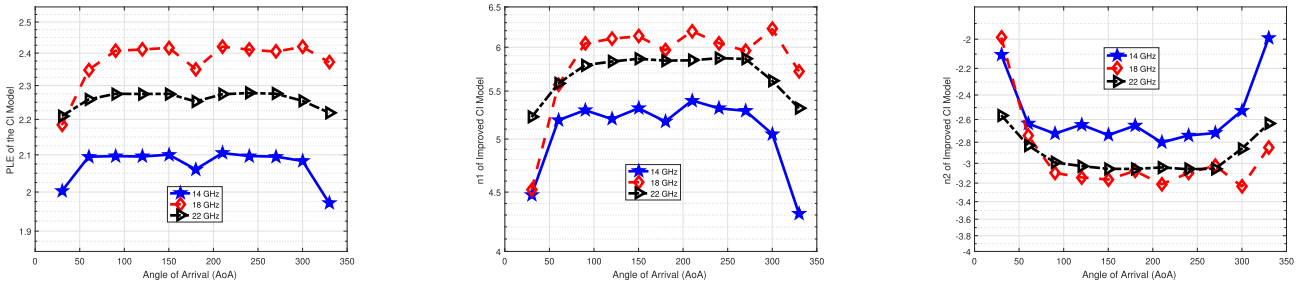

(a) The PLE of the CI model. (b) n_1 of the improved CI model. (c) n_2 of the improved CI model.

FIGURE 8. **The behavior of the CI and improved CI models' parameters with the AoA.**

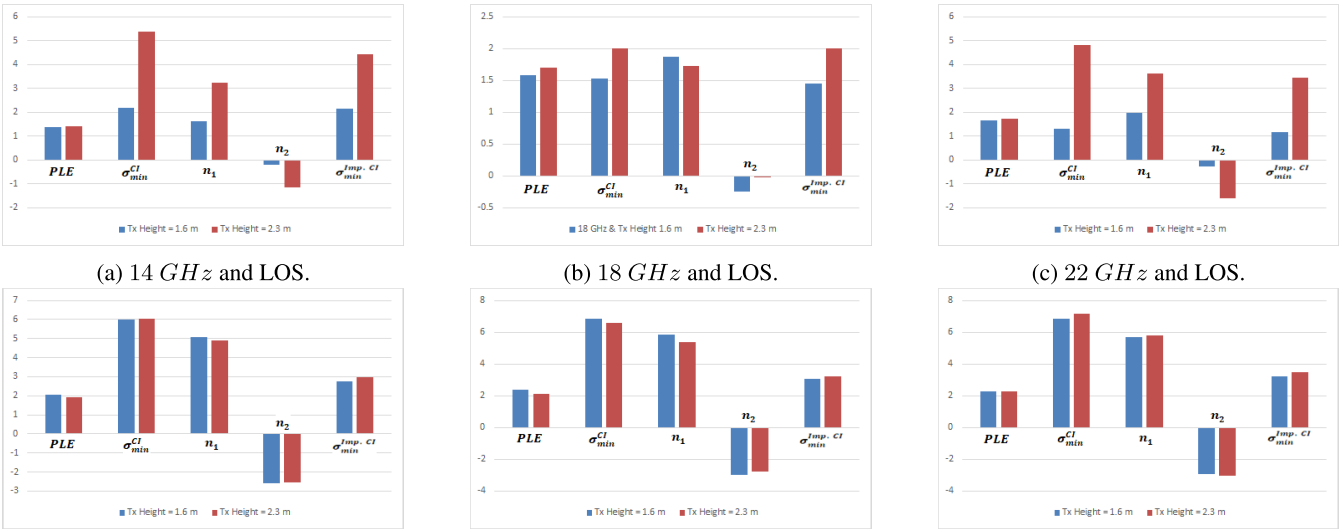

(a) 14 GHz and LOS. (b) 18 GHz and LOS. (c) 22 GHz and LOS.

(d) 14 GHz and NLOS. (e) 18 GHz and NLOS. (f) 22 GHz and NLOS.

FIGURE 9. **The parameters of the CI and improved-CI models at two different Tx antenna heights.**

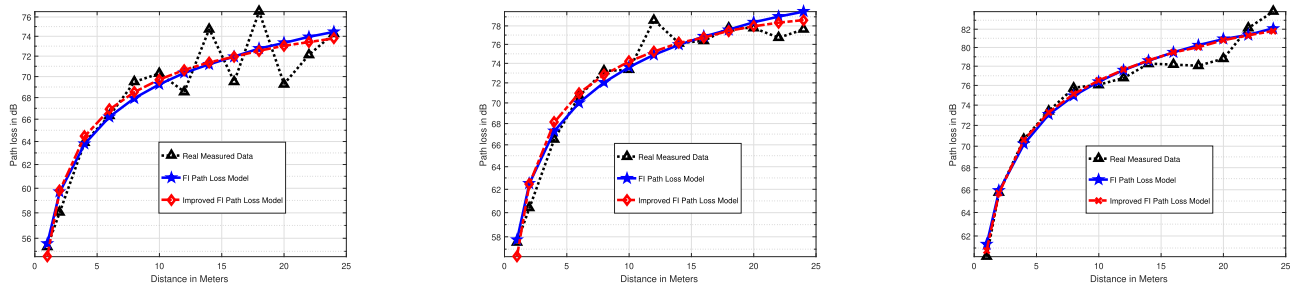

(a) $f = 14\,GHz$. (b) $f = 18\,GHz$. (c) $f = 22\,GHz$.

FIGURE 10. **Comparison of measured path loss, the fitted FI model, and the improved FI model for the LOS results at 14, 18, and 22 *GHz*.**

propagation characteristics caused by the mismatching of the Tx and Rx antenna heights. Furthermore, it reveals that the antenna height's impact is minimum at 22 GHz and maximum at 14 GHz for both the CI model and our proposed model. However, when we look at the SF's standard deviation values, we observe that the proposed model outperforms the standard CI model depending on the antennas' heights. It is worth noting that the antenna height might not be an essential factor in the specific investigations presented in this work. However, the antenna locations, patterns, and relative orientation are significant factors, especially at high frequencies, mmWave and above. These performance studies will help engineers in designing reliable communication systems in such scenarios and have an accurate understanding and modeling of the wireless channel's behavior.

B. RESULTS AND DISCUSSIONS OF COMPARING THE FI WITH IMPROVED-FI MODELS

Fig. 10 shows the curves of the real measured data, the FI model, and the improved-FI model for the LOS

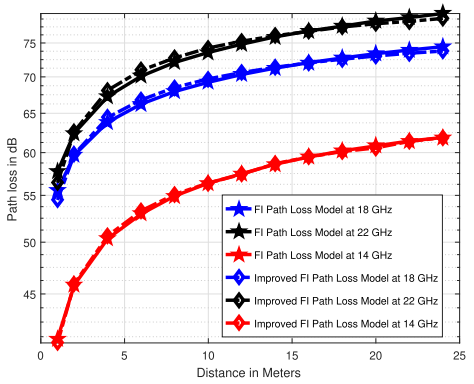

FIGURE 11. Directional large-scale path loss prediction models for the LOS communication scenario.

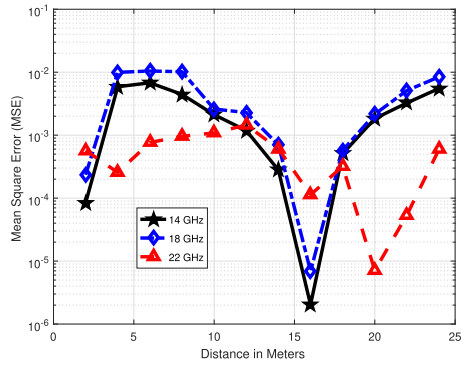

FIGURE 12. MSE between the FI and improved FI models in the LOS communication scenario.

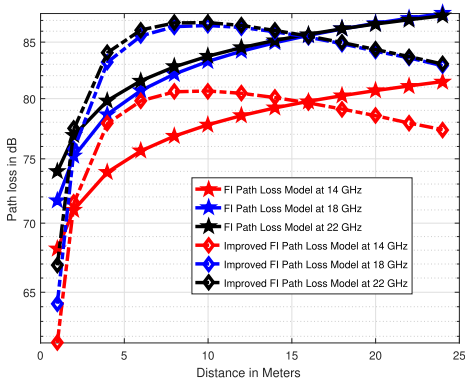

FIGURE 13. Directional large-scale path loss prediction models for the NLOS communication scenario.

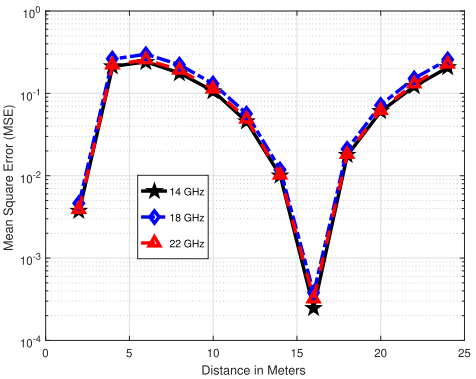

FIGURE 14. MSE between the FI and improved FI models in the NLOS communication scenario.

TABLE 7. A comparison between the FI and Improved-FI models' parameters in the LOS scenario.

	$14\,GHz$	$18\,GHz$	$22\,GHz$
$\alpha_{FI}[dB]$	55.443	57.478	61.036
β_{FI}	1.365	1.590	1.503
$\sigma^{FI}_{min}[dB]$	2.19	1.53	1.12
$\alpha_{Imp.FI}[dB]$	54.410	56.136	60.652
$\beta_1^{Imp.FI}$	1.827	2.191	1.675
$\beta_2^{Imp.FI}$	−0.315	−0.409	−0.117
$\sigma^{Imp.FI}_{min}[dB]$	2.12	1.38	1.10

communication scenario at the three frequency bands adopted for this work. The figure shows that both models accurately fit the real measured data with the minimum possible MSE between the models and the data. As a comparison between the three frequencies, the best fit occurs at the 22 *GHz* frequency band. It must be emphasized that any path loss model will always depend on the operating frequency, no matter how they are derived. Maybe simplifications could come from the fact that the exact carrier frequency is not needed, and only the knowledge of the band (e.g., 14 *GHz*, 18 *GHz*, and 22 *GHz*) is enough. The models' parameters are represented in Table 7. It is observed that our proposed model slightly betters the standard FI model in terms of the performance since it reduces the standard deviation values by 3.2%, 13.7%, and 1.8% at 14, 18, and 22 *GHz*. Note that the best improvement applies at 18 *GHz*, contrary to what happened between the CI and improved-CI models. Also, note that the values of the parameter α are not far between both models. A notable improvement can be observed from Table 8 since the percentage reduction goes up to 44% in the NLOS communication scenario. Upon comparing the four models, it is noted that the best model that fits the real measured data is the improved-FI model. Fig. 11 presents both FI and improved-FI models together at the three frequencies selected. The curves of the two models in the figure are almost the same, as also confirmed from the values in Table 7. We have plotted the MSE between both models to show how these models behave when the Tx-Rx separation distance increases. It is noted that from Fig. 12, the correlation between the models is high since the values of the MSE are in the range of 10^{-6} and 10^{-2} with minimum values around the breakpoint. Nevertheless, Fig. 13 and Fig. 14 show a highly notable difference between both models in terms of their performance in the NLOS scenario since the models' curves are far away from each other in Fig. 13, and have MSE values higher than the ones we got from Fig. 12.

Fig. 15 represents the FI and improved-FI models' parameters versus the AoA of the receiving antenna at 14, 18, and 22 *GHz* for the NLOS communication scenario. This figure shows that while both models provide a valuable stability to the change of the AoA, our proposed model shows slight advantage. This advantage is seen clearly from Tables 9, 10, and 11, where the models' parameters are presented. The impact of the antenna heights on the models'

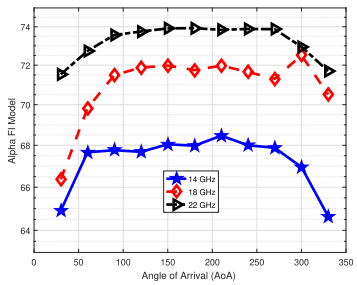

(a) α of the FI model.

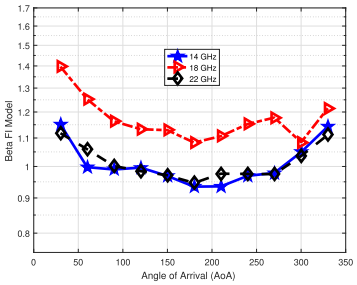

(b) β of the FI model.

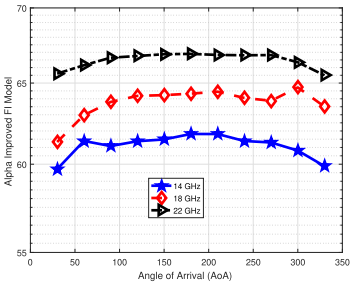

(c) α of the improved FI model.

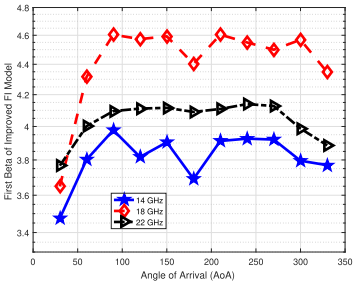

(d) β_1 of the improved FI model.

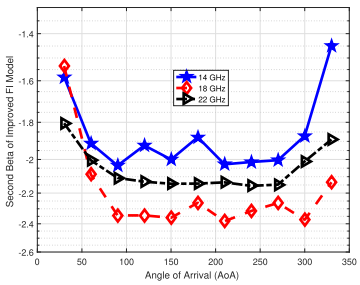

(e) β_2 of the improved FI model.

FIGURE 15. The behavior of the FI and improved FI models' parameters with the AoA.

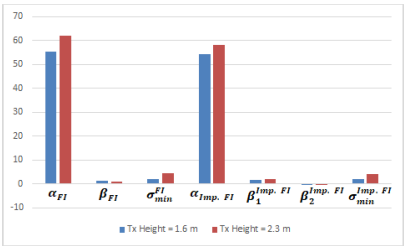

(a) 14 GHz and LOS.

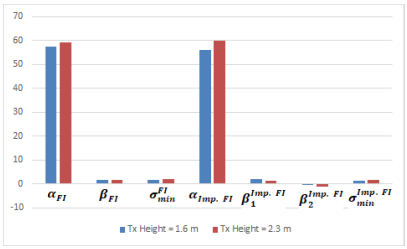

(b) 18 GHz and LOS.

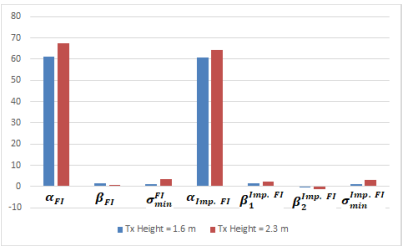

(c) 22 GHz and LOS.

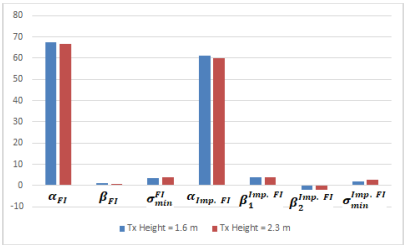

(d) 14 GHz and NLOS.

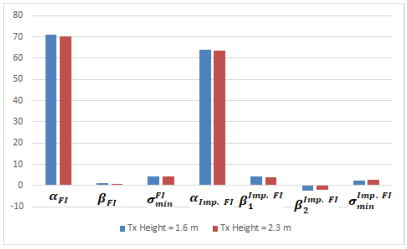

(e) 18 GHz and NLOS.

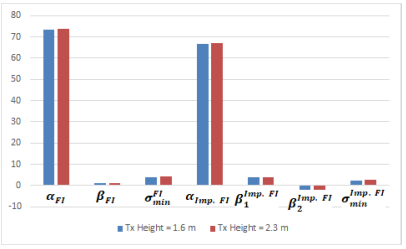

(f) 22 GHz and NLOS.

FIGURE 16. The parameters of the FI and improved-FI models at two different Tx antenna heights.

TABLE 8. A comparison between the FI and Improved-FI models' parameters in the NLOS scenario.

	14 GHz	18 GHz	22 GHz
$\alpha_{FI}[dB]$	67.272	71.021	73.242
β_{FI}	1.010	1.172	1.014
$\sigma^{FI}_{min}[dB]$	3.69	4.32	4.07
$\alpha_{Imp.FI}[dB]$	61.097	63.767	66.476
$\beta_1^{Imp.FI}$	3.772	4.430	4.039
$\beta_2^{Imp.FI}$	−1.881	−2.218	−2.061
$\sigma^{Imp.FI}_{min}[dB]$	2.10	2.42	2.36

parameters is presented in Fig. 16. As for the behavior of the CI model and the proposed improved version, when there is a change in the antenna's height, there will be a corresponding change in the models' parameters, and the worst behavior is seen to occur when there is a mismatch in the antenna's heights. However, the performance of our proposed model is better than the performance of the standard FI model.

From the previous analysis, we observed that it is possible to provide valuable improvements to the existing wireless channel models without a notable increase in the models' complexity. In fact, with the demand for more and more data traffic, we will always need to go for higher frequency bands to meet future requirements. These higher frequency bands have smaller wavelengths, they then suffer more from the wireless propagation channel. Hence, improving the existing

TABLE 9. The behavior of the FI and Improved-FI models' parameters with the AoA at 14 *GHz* frequency band.

	30°	60°	90°	120°	150°	180°	210°	240°	270°	300°	330°
$\alpha_{FI}[dB]$	64.907	67.663	67.766	67.683	68.051	67.981	68.470	68.003	67.879	66.954	64.638
β_{FI}	1.151	0.998	0.990	0.996	0.969	0.935	0.936	0.969	0.979	1.049	1.143
$\sigma^{FI}_{min}[dB]$	2.86	3.82	3.88	3.83	3.97	3.96	4.13	3.95	3.91	3.56	2.76
$\alpha_{Imp.FI}[dB]$	59.709	61.391	61.084	61.376	61.484	61.816	61.813	61.390	61.300	60.813	59.882
$\beta_1^{Imp.FI}$	3.475	3.802	3.977	3.817	3.905	3.691	3.912	3.926	3.921	3.795	3.269
$\beta_2^{Imp.FI}$	−1.58	−1.91	−2.03	−1.92	−2.01	−1.88	−2.03	−2.01	−2.01	−1.87	−1.45
$\sigma^{Imp.FI}_{min}[dB]$	1.29	2.26	2.07	2.26	2.33	2.55	2.53	2.26	2.20	1.89	1.47

TABLE 10. The behavior of the FI and Improved-FI models' parameters with the AoA at 18 *GHz* frequency band.

	30°	60°	90°	120°	150°	180°	210°	240°	270°	300°	330°
$\alpha_{FI}[dB]$	66.368	69.824	71.492	71.878	71.977	71.749	71.974	71.653	71.301	72.513	70.507
β_{FI}	1.397	1.253	1.163	1.133	1.129	1.083	1.107	1.153	1.178	1.085	1.215
$\sigma^{FI}_{min}[dB]$	2.71	3.86	4.47	4.61	4.65	4.58	4.76	4.52	4.39	4.85	4.11
$\alpha_{Imp.FI}[dB]$	61.330	62.972	63.796	64.183	64.230	64.325	64.449	64.055	63.873	64.721	63.503
$\beta_1^{Imp.FI}$	3.649	4.316	4.604	4.573	4.592	4.402	4.604	4.549	4.499	4.568	4.346
$\beta_2^{Imp.FI}$	−1.53	−2.09	−2.34	−2.34	−2.36	−2.26	−2.38	−2.31	−2.26	−2.37	−2.13
$\sigma^{Imp.FI}_{min}[dB]$	1.11	1.89	2.40	2.65	2.68	2.77	2.82	2.57	2.45	2.99	2.24

TABLE 11. The behavior of the FI and Improved-FI models' parameters with the AoA at 22 *GHz* frequency band.

	30°	60°	90°	120°	150°	180°	210°	240°	270°	300°	330°
$\alpha_{FI}[dB]$	71.531	72.732	73.565	73.751	73.910	73.927	73.836	73.883	73.871	72.949	71.703
β_{FI}	1.118	1.059	1.002	0.985	0.971	0.946	0.976	0.976	0.975	1.036	1.112
$\sigma^{FI}_{min}[dB]$	3.43	3.88	4.19	4.27	4.33	4.33	4.30	4.32	4.31	3.96	3.50
$\alpha_{Imp.FI}[dB]$	65.606	66.151	66.646	66.758	66.876	66.896	66.829	66.806	66.819	66.347	65.498
$\beta_1^{Imp.FI}$	3.767	4.001	4.095	4.111	4.115	4.090	4.108	4.139	4.127	3.987	3.886
$\beta_2^{Imp.FI}$	−1.80	−2.00	−2.10	−2.13	−2.14	−2.14	−2.13	−2.15	−2.14	−2.01	−1.88
$\sigma^{Imp.FI}_{min}[dB]$	1.82	2.15	2.47	2.54	2.61	2.63	2.58	2.56	2.57	2.28	1.74

models and developing new models that accurately describe the wireless propagation channel will always be needed.

V. CONCLUSION

In this paper, a simple and efficient improvement of two well-known path loss prediction models, namely the CI and FI models, was presented and discussed in detail. The validation of the models' performance was given by applying the CI and FI models and their improvement to fit real measured data. The data was collected in a typical indoor corridor environment at three frequencies in the SHF band, which are 14, 18, and 22 *GHz*. Both the LOS and NLOS communication scenarios were considered in this research. The main findings of this work are that our proposed models generally outperform the existing standard models in terms of several factors such as the accuracy of predicting the path loss with the lowest possible value of the MSE, minimizing the SF's standard deviation for both LOS and NLOS conditions (with better improvements in the NLOS scenario), and providing better sensitivity and stability of the models' parameters with the change of the AoA and antenna height. The improvement of the models was effected through a simple and valuable approach. There is no notable increase in the models' complexity to be used by the planning engineers for wireless systems' deployment and calculations of the link budget. Finally, this work shows that the proposed models can be trusted as accurate and reliable models for predicting the path loss at frequency bands above 6 *GHz* in enclosed indoor environments such as corridors since they provide better accuracy, sensitivity, and stability than well-known standard path loss prediction models such as the CI and FI models. Further studies and investigations need to be conducted to achieve greater accuracy in predicting the path loss since it is the dominant component that determines the networks' overall coverage.

REFERENCES

[1] E. Basar, M. Di Renzo, J. De Rosny, M. Debbah, M. Alouini, and R. Zhang, "Wireless communications through reconfigurable intelligent surfaces," *IEEE Access*, vol. 7, pp. 116753–116773, 2019.

[2] (Feb. 2019). *Cisco Visual Networking Index: Global Mobile Data Traffic Forecast Update, 2017–2022*. [Online]. Available: https://www.cisco.com/c/en/us/solutions/collateral/serviceprovider/visual-networking-index-vni/white-paper-c11-738429.pdf

[3] N. O. Oyie and T. J. O. Afullo, "Measurements and analysis of large-scale path loss model at 14 and 22 GHz in indoor corridor," *IEEE Access*, vol. 6, pp. 17205–17214, 2018.

[4] X. Wu, C. X. Wang, J. Sun, J. Huang, R. Feng, Y. Yang, and X. Ge, "60-GHz millimeter-wave channel measurements and modeling for indoor office environments," *IEEE Trans. Antennas Propag.*, vol. 65, no. 4, pp. 1912–1924, Apr. 2017.

[5] T. S. Rappaport, G. R. Maccartney, M. K. Samimi, and S. Sun, "Wideband millimeter-wave propagation measurements and channel models for future wireless communication system design," *IEEE Trans. Commun.*, vol. 63, no. 9, pp. 3029–3056, Sep. 2015.

[6] P. F. M. Smulders, "Statistical characterization of 60-GHz indoor radio channels," *IEEE Trans. Antennas Propag.*, vol. 57, no. 10, pp. 2820–2829, Oct. 2009.

[7] L. Pometcu and R. D'Errico, "An indoor channel model for high data-rate communications in D-band," *IEEE Access*, vol. 8, pp. 9420–9433, 2020.

[8] A. Osseiran, J. F. Monserratand, and P. Marsch, "5G mobile and wireless communications technology," *Int. J. Satell. Commun. Networ.*, vol. 34, no. 3, pp. 351–360, May 2016.

[9] M. Aborahama, A. Zakaria, M. H. Ismail, M. El-Bardicy, M. El-Tarhuni, and Y. Hatahet, "Large-scale channel characterization at 28 GHz on a university campus in the United Arab Emirates," *Telecommun. Syst.*, vol. 1, pp. 1–15, Jan. 2020.

[10] M. K. Elmezughi, T. J. Afullo, and N. O. Oyie, "Performance study of path loss models at 14, 18, and 22 GHz in an indoor corridor environment for wireless communications," *SAIEE Afr. Res. J.*, vol. 112, no. 1, pp. 32–45, Mar. 2021.
[11] T. S. Rappaport, S. Sun, R. Mayzus, H. Zhao, Y. Azar, K. Wang, G. N. Wong, J. K. Schulz, M. Samimi, and F. Gutierrez, "Millimeter wave mobile communications for 5G cellular: It will work!" *IEEE Access*, vol. 1, pp. 335–349, 2013.
[12] A. Zhou, J. Huang, J. Sun, Q. Zhu, C.-X. Wang, and Y. Yang, "60 GHz channel measurements and ray tracing modeling in an indoor environment," in *Proc. 9th Int. Conf. Wireless Commun. Signal Process. (WCSP)*, Oct. 2017, pp. 3029–3056.
[13] G. R. MacCartney, H. Yan, S. Sun, and T. S. Rappaport, "A flexible wideband millimeter-wave channel sounder with local area and NLOS to LOS transition measurements," in *Proc. IEEE Int. Conf. Commun. (ICC)*, May 2017, pp. 1–7.
[14] C.-L. Cheng, S. Kim, and A. Zajic, "Comparison of path loss models for indoor 30 GHz, 140 GHz, and 300 GHz channels," in *Proc. 11th Eur. Conf. Antennas Propag. (EUCAP)*, Mar. 2017, pp. 716–720.
[15] A. M. Al-samman, T. A. A. Rahman, M. H. Azmi, and S. A. Al-Gailani, "Millimeter-wave propagation measurements and models at 28 GHz and 38 GHz in a dining room for 5G wireless networks," *Measurement*, vol. 130, pp. 71–81, Dec. 2018.
[16] M. K. Elmezughi, T. J. Afullo, and N. O. Oyie, "Investigating the impact of antenna heights on path loss models in an indoor corridor environment," in *Proc. Int. Conf. Artif. Intell., Big Data, Comput. Data Commun. Syst. (icABCD)*, Aug. 2020, pp. 1–7.
[17] F. Hossain, T. Geok, T. Rahman, M. Hindia, K. Dimyati, and A. Abdaziz, "Indoor millimeter-wave propagation prediction by measurement and ray tracing simulation at 38 GHz," *Symmetry*, vol. 10, no. 10, p. 464, Oct. 2018.
[18] T. Kleine-Ostmann, C. Jastrow, S. Priebe, M. Jacob, T. Kurner, and T. Schrader, "Measurement of channel and propagation properties at 300 GHz," in *Proc. Conf. Precis. Electromagn. Meas.*, Jul. 2012, pp. 258–259.
[19] A. Gatherer. *What Will 6G be*. [Online]. Available: https://www.comsoc.org/publications/ctn/what-will-6g-be
[20] M. K. Samimi, T. S. Rappaport, and G. R. MacCartney, Jr., "Probabilistic omnidirectional path loss models for millimeter-wave outdoor communications," *IEEE Wireless Commun. Lett.*, vol. 4, no. 4, pp. 357–360, Aug. 2015.
[21] N. A. Muhammad, P. Wang, Y. Li, and B. Vucetic, "Analytical model for outdoor millimeter wave channels using geometry-based stochastic approach," *IEEE Trans. Veh. Technol.*, vol. 66, no. 2, pp. 912–926, Feb. 2017.
[22] Z. Pi and F. Khan, "An introduction to millimeter-wave mobile broadband systems," *IEEE Commun. Mag.*, vol. 49, no. 6, pp. 101–107, Jun. 2011.
[23] G. R. Maccartney, T. S. Rappaport, S. Sun, and S. Deng, "Indoor office wideband millimeter-wave propagation measurements and channel models at 28 and 73 GHz for ultra-dense 5G wireless networks," *IEEE Access*, vol. 3, pp. 2388–2424, 2015.
[24] A. M. Al-Samman, M. N. Hindia, and T. A. Rahman, "Path loss model in outdoor environment at 32 GHz for 5G system," in *Proc. IEEE 3rd Int. Symp. Telecommun. Technol. (ISTT)*, Nov. 2016, pp. 9–13.
[25] M. N. Hindia, A. M. Al-Samman, and T. Bin Abd Rahman, "Investigation of large-scale propagation for outdoor-parking lot environment for 5G wireless communications," in *Proc. IEEE 3rd Int. Symp. Telecommun. Technol. (ISTT)*, Nov. 2016, pp. 14–18.
[26] D. Chizhik, J. Du, R. Feick, M. Rodriguez, G. Castro, and R. A. Valenzuela, "Path loss and directional gain measurements at 28 GHz for non-line-of-sight coverage of indoors with corridors," *IEEE Trans. Antennas Propag.*, vol. 68, no. 6, pp. 4820–4830, Jun. 2020.
[27] S. Sun, T. S. Rappaport, S. Rangan, T. A. Thomas, A. Ghosh, I. Z. Kovacs, I. Rodriguez, O. Koymen, A. Partyka, and J. Jarvelainen, "Propagation path loss models for 5G urban Micro- and macro-cellular scenarios," in *Proc. IEEE 83rd Veh. Technol. Conf. (VTC Spring)*, May 2016, pp. 1–6.
[28] A. M. Al-Samman, T. A. Rahman, T. Al-Hadhrami, A. Daho, M. N. Hindia, M. H. Azmi, K. Dimyati, and M. Alazab, "Comparative study of indoor propagation model below and above 6 GHz for 5G wireless networks," *Electronics*, vol. 8, no. 1, p. 44, Jan. 2019.
[29] M. B. Majed, T. A. Rahman, O. A. Aziz, M. N. Hindia, and E. Hanafi, "Channel characterization and path loss modeling in indoor environment at 4.5, 28, and 38 GHz for 5G cellular networks," *Int. J. Antennas Propag.*, vol. 2018, pp. 1–14, Sep. 2018.
[30] A. I. Sulyman, A. Alwarafy, H. E. Seleem, K. Humadi, and A. Alsanie, "Path loss channel models for 5G cellular communications in Riyadh city at 60 GHz," in *Proc. IEEE Int. Conf. Commun. (ICC)*, May 2016, pp. 1–6.
[31] N. R. Zulkefly, T. A. Rahman, M. H. Azmi, and O. A. Aziz, "6.5 GHz and 10.2 GHz path loss measurements and modeling for 5G communications system prediction," *Int. J. Res. Eng. Technol.*, vol. 6, no. 11, pp. 6–11, Nov. 2017.
[32] M. Khalily, M. Ghoraishi, S. Taheri, S. Payami, and R. Tafazolli, "Millimeter-wave directional path loss models in the 26 GHz, 32 GHz, and 39 GHz bands for small cell 5G cellular system," in *Proc. 12th Eur. Conf. Antennas Propag. (EuCAP)*, 2018, pp. 5–17.
[33] A. M. Al-Samman, T. A. Rahman, N. Hindia, and J. Nasir, "Path loss model for indoor emergency stairwell environment at millimeter wave band for 5G network," *Turkish J. Electr. Eng. Comput. Sci.*, vol. 26, no. 6, pp. 3024–3032, Nov. 2018.
[34] A. Al-Samman, T. Rahman, M. Hindia, A. Daho, and E. Hanafi, "Path loss model for outdoor parking environments at 28 GHz and 38 GHz for 5G wireless networks," *Symmetry*, vol. 10, no. 12, p. 672, Nov. 2018.
[35] G. R. Maccartney, T. S. Rappaport, M. K. Samimi, and S. Sun, "Millimeter-wave omnidirectional path loss data for small cell 5G channel modeling," *IEEE Access*, vol. 3, pp. 1573–1580, 2015.
[36] A. M. Al-samman, T. Abd Rahman, and M. H. Azmi, "Indoor corridor wideband radio propagation measurements and channel models for 5G millimeter wave wireless communications at 19 GHz, 28 GHz, and 38 GHz bands," *Wireless Commun. Mobile Comput.*, vol. 2018, pp. 1–12, Mar. 2018.
[37] H. A. Obeidat, R. Asif, N. T. Ali, Y. A. Dama, O. A. Obeidat, S. M. R. Jones, W. S. Shuaieb, M. A. Al-Sadoon, K. W. Hameed, A. A. Alabdullah, and R. A. Abd-Alhameed, "An indoor path loss prediction model using wall correction factors for wireless local area network and 5G indoor networks," *Radio Sci.*, vol. 53, no. 4, pp. 544–564, Apr. 2018.
[38] T. O. Olasupo, C. E. Otero, L. D. Otero, K. O. Olasupo, and I. Kostanic, "Path loss models for low-power, low-data rate sensor nodes for smart car parking systems," *IEEE Trans. Intell. Transp. Syst.*, vol. 19, no. 6, pp. 1774–1783, Jun. 2018.
[39] S. Sun, T. S. Rappaport, T. A. Thomas, A. Ghosh, H. C. Nguyen, I. Z. Kovács, I. Rodriguez, O. Koymen, and A. Partyka, "Investigation of prediction accuracy, sensitivity, and parameter stability of large-scale propagation path loss models for 5G wireless communications," *IEEE Trans. Veh. Technol.*, vol. 65, no. 5, pp. 2843–2860, May 2016.
[40] A. Al-Hourani and K. Gomez, "Modeling cellular-to-UAV path-loss for suburban environments," *IEEE Wireless Commun. Lett.*, vol. 7, no. 1, pp. 82–85, Feb. 2018.
[41] D. Casillas-Perez, C. Camacho-Gomez, S. Jimenez-Fernandez, J. A. Portilla-Figueras, and S. Salcedo-Sanz, "Weighted ABG: A general framework for optimal combination of ABG path-loss propagation models," *IEEE Access*, vol. 8, pp. 101758–101769, Jun. 2020.
[42] S. Kaddouri, M. E. Hajj, G. Zaharia, and G. E. Zein, "Indoor path loss measurements and modeling in an open-space office at 2.4 GHz and 5.8 GHz in the presence of people," in *Proc. IEEE 29th Annu. Int. Symp. Pers., Indoor Mobile Radio Commun. (PIMRC)*, Sep. 2018, pp. 1–7.
[43] C. U. Kumari, P. Kora, K. Meenakshi, and S. K., "Short term and long term path loss estimation in urban, Suburban and rural areas," in *Proc. 3rd Int. Conf. Comput. Methodolog. Commun. (ICCMC)*, Mar. 2019, pp. 114–117.
[44] J.-H. Lee, J.-S. Choi, and S.-C. Kim, "Cell coverage analysis of 28 GHz millimeter wave in urban microcell environment using 3-D ray tracing," *IEEE Trans. Antennas Propag.*, vol. 66, no. 3, pp. 1479–1487, Mar. 2018.
[45] J. R. Perez, R. P. Torres, L. Rubio, J. Basterrechea, M. Domingo, V. M. R. Penarrocha, and J. Reig, "Empirical characterization of the indoor radio channel for array antenna systems in the 3 to 4 GHz frequency band," *IEEE Access*, vol. 7, pp. 94725–94736, 2019.
[46] K. Haneda *et al.*, "5G 3GPP-like channel models for outdoor urban microcellular and macrocellular environments," in *Proc. IEEE 83rd Veh. Technol. Conf. (VTC Spring)*, May 2016, pp. 1–7.
[47] K. Haneda *et al.*, "Indoor 5G 3GPP-like channel models for office and shopping mall environments," in *Proc. IEEE Int. Conf. Commun. Workshops (ICC)*, May 2016, pp. 694–699.
[48] S. Sun, G. R. MacCartney, and T. S. Rappaport, "Millimeter-wave distance-dependent large-scale propagation measurements and path loss models for outdoor and indoor 5G systems," in *Proc. 10th Eur. Conf. Antennas Propag. (EuCAP)*, Apr. 2016, pp. 1–5.
[49] M. Ozpolat, K. Bhargava, E. Kampert, and M. D. Higgins, "Multi-lane urban mmWave V2V networks: A path loss behaviour dependent coverage analysis," *Veh. Commun.*, vol. 30, pp. 2096–2214, Mar. 2021.

[50] N. O. Oyie and T. J. O. Afullo, "A comparative study of dual-slope path loss model in various indoor environments at 14 to 22 GHz," in *Proc. Prog. Electromagn. Res. Symp.*, Aug. 2018, pp. 121–128.
[51] A. I. Sulyman, A. T. Nassar, M. K. Samimi, G. R. MacCartney, Jr., T. S. Rappaport, and A. Alsanie, "Radio propagation path loss models for 5G cellular networks in the 28 GHz and 38 GHz millimeter-wave bands," *IEEE Commun. Mag.*, vol. 52, no. 9, pp. 78–86, Sep. 2014.
[52] G. R. MacCartney and T. S. Rappaport, "Rural macrocell path loss models for millimeter wave wireless communications," *IEEE J. Sel. Areas Commun.*, vol. 35, no. 7, pp. 1663–1677, Jul. 2017.
[53] S. Hur, S. Baek, B. Kim, Y. Chang, A. F. Molisch, T. S. Rappaport, K. Haneda, and J. Park, "Proposal on millimeter-wave channel modeling for 5G cellular system," *IEEE J. Sel. Topics Signal Process.*, vol. 10, no. 3, pp. 454–469, Apr. 2016.
[54] M. Cheffena and M. Mohamed, "Empirical path loss models for wireless sensor network deployment in snowy environments," *IEEE Antennas Wireless Propag. Lett.*, vol. 16, pp. 2877–2880, Sep. 2017.
[55] A. M. Al-Samman, T. A. Rahman, M. Hadri, and M. N. Hindia, "Path loss and RMS delay spread model for 5G channel at 19 GHz," in *Proc. IEEE 13th Int. Colloq. Signal Process. Appl. (CSPA)*, Mar. 2017, pp. 49–54.
[56] A. M. Al-Samman, T. A. Rahman, M. H. Azmi, A. Sharaf, Y. Yamada, and A. Alhammadi, "Path loss model in indoor environment at 40 GHz for 5G wireless network," in *Proc. IEEE 14th Int. Colloq. Signal Process. Appl. (CSPA)*, Mar. 2018, pp. 7–12.
[57] S. Deng, G. R. MacCartney, and T. S. Rappaport, "Indoor and outdoor 5G diffraction measurements and models at 10, 20, and 26 GHz," in *Proc. IEEE Global Commun. Conf. (GLOBECOM)*, Dec. 2016, pp. 1–7.
[58] M. Khatun, H. Mehrpouyan, and D. Matolak, "60-GHz millimeter-wave pathloss measurements in boise airport," in *Proc. IEEE Global Conf. Signal Inf. Process. (GlobalSIP)*, Nov. 2018, pp. 1276–1280.
[59] H. Zhao, Q. Wang, and K. Shi, "Analysis on human blockage path loss and shadow fading in millimeter-wave band," *Int. J. Antennas Propag.*, vol. 2017, pp. 1–6, Jan. 2017.
[60] O. Ahmadien, H. F. Ates, T. Baykas, and B. K. Gunturk, "Predicting path loss distribution of an area from satellite images using deep learning," *IEEE Access*, vol. 8, pp. 64982–64991, 2020.
[61] A. Alwarafy, A. I. Sulyman, A. Alsanie, S. A. Alshebeili, and H. M. Behairy, "Path-loss channel models for receiver spatial diversity systems at 2.4 GHz," *Int. J. Antennas Propag.*, vol. 2017, pp. 1–12, Jan. 2017.
[62] M. Laskowski, S. J. Ambroziak, L. M. Correia, and K. Swider, "On the usefulness of the Generalised additive model for mean path loss estimation in body area networks," *IEEE Access*, vol. 8, pp. 176873–176882, 2020.
[63] L. Rubio, J. Reig, H. Fernández, and V. M. Rodrigo-Peñarrocha, "Experimental UWB propagation channel path loss and time-dispersion characterization in a laboratory environment," *Int. J. Antennas Propag.*, vol. 2013, pp. 1–7, Mar. 2013.
[64] L. Wu, D. He, B. Ai, J. Wang, H. Qi, K. Guan, and Z. Zhong, "Artificial neural network based path loss prediction for wireless communication network," *IEEE Access*, vol. 8, pp. 199523–199538, 2020.
[65] Y. Xing and T. S. Rappaport, "Propagation measurements and path loss models for sub-THz in urban microcells," 2021, *arXiv:2103.01151*. [Online]. Available: http://arxiv.org/abs/2103.01151
[66] Y. Xing, T. S. Rappaport, and A. Ghosh, "Millimeter wave and sub-THz indoor radio propagation channel measurements, models, and comparisons in an office environment," *IEEE Commun. Lett.*, early access, Jun. 10, 2021, doi: 10.1109/LCOMM.2021.3088264.

MOHAMED K. ELMEZUGHI (Student Member, IEEE) was born in Tripoli, Libya, in 1995. He received the bachelor's degree (Hons.) in electrical engineering from the University of Tripoli, Libya, in 2017, and the master's degree *(cum laude)* in electronic engineering from the University of KwaZulu-Natal (UKZN), Durban, South Africa, in 2020, where he is currently pursuing the Ph.D. degree under the supervision of Prof. Thomas J. Afullo. The focus of his Ph.D. research is on millimeter-wave channel modeling for 5G mobile communication systems and beyond. His research interests include millimeter-wave systems, wireless channel modeling, signal detection, antennas design, radio propagation, and channel parameters estimation.

THOMAS J. AFULLO (Senior Member, IEEE) received the B.Sc. degree (Hons.) in electrical engineering from the University of Nairobi, Kenya, in 1979, the M.S.E.E. degree through a Fulbright-Hays Scholarship from West Virginia University, Morgantown, USA, in 1983, and the Bijzondre License in Technology and the Ph.D. degree in telecommunication engineering from Vrije Universiteit Brussel (VUB), Belgium, in 1989. From 1979 to 1986, he promoted from a rank of a Pupil (Trainee) Engineer to a Senior Executive Engineer in charge of transmission and radio planning with Kenya Posts and Telecommunication Corporation. From 1987 to 1994, he promoted from a rank of a Tutorial Fellow to a Senior Lecturer and the Head of the Department of Electrical and Communications Engineering, Moi University, Eldoret, Kenya. From 1996 to 2002, he was a Lecturer in telecommunication with the Department of Electrical Engineering, University of Botswana, Gaborone. He joined the University of Durban-Westville, as an Associate Professor of electrical engineering, in 2003. Since 2012, he has been a Professor of telecommunications engineering with the Discipline of Electrical, Electronic and Computer Engineering, University of KwaZulu-Natal (UKZN), Durban. He is also the Director of the Telkom Centre for Radio Access & Rural Technologies (CRART). He has spent Sabbatical Leave with Prof. Emilio Matriciani and Prof. Carlo Riva with Politechnico di Milano (POLIMI), in 2017, with Prof. Rajarathnam Chandramouli with Stevens Institute of Technology, New Jersey, in 2017, and the Department of Electronics, University of Kaiserslautern, Germany, in 1996, on a DAAD Fellowship. He has successfully supervised 16 Ph.D. and 28 master's students, as well as co-supervised two Ph.D. students. His research interests include microwave and millimeter-wave propagation, power line communications (PLC), and free space optics (FSO). He is a Registered Engineer with the Engineering Council of South Africa (ECSA). He is a fellow of the South African Institute of Electrical Engineering (SAIEE), and a Rated Researcher with the South African National Research Foundation (NRF). He was a member of Eta-Kappa Nu (Beta-Rho Chapter), in 1982. Since 2016, he has been a Faculty Advisor and a member of the IEEE-Eta-Kappa Nu (Mu Eta Chapter).